Available online at www.sciencedirect.com

SciVerse ScienceDirect

Ceramics International 39 (2013) 6923–6929

CERAMICS INTERNATIONAL

www.elsevier.com/locate/ceramint

Morphology control and improved field emission properties of ZnO tetrapod films deposited by electrophoretic deposition

L.A. Ma[a,*], T.L. Guo[b]

[a]School of materials science and Engineering, Fujian University of Technology, Fuzhou 350108, PR China
[b]Institutes of Optoelectronics and Displays Technology, Fuzhou University, Fuzhou 350002, PR China

Received 9 November 2012; received in revised form 12 February 2013; accepted 12 February 2013
Available online 20 February 2013

Abstract

High-quality ZnO tetrapods with different morphologies were synthesized via thermal evaporation of a surface-modified Zn powder in an oxygen/argon mixed gas. The morphology, including the size and shape of the individual legs of ZnO tetrapods, was, easily altered by adjusting the proportion of oxygen in the carrier gas and the reaction temperature of the furnace. A correlation between the experimental parameters and the product morphologies was proposed and discussed. Moreover, the influence of the deposition time on the field emission (FE) characteristics of ZnO-tetrapod cathodes fabricated by the electrophoretic deposition (EPD) method was investigated. The results show that ZnO-tetrapod cathodes grown for 15 min have the best field emission properties, with a turn-on field of 2.01 V/μm, a threshold field of ~3.8 V/μm, a current density of 1.96 mA/cm^2 at a field of ~4.62 V/μm, and a field enhancement factor as high as 1.1×10^4. The low threshold field and marked enhancement in β were attributed to the small radius of curvature, the high aspect ratio, and, perhaps more importantly, the proper density distribution of ZnO tetrapods.

Keywords: D. ZnO; Thermal evaporation; Electrophoretic deposition; Field emission

1. Introduction

Semiconductor nanostructures have been attracting increasing attention due to their exceptional properties, which are different from those of bulk materials. As ZnO is a direct wide band gap (3.37 eV) semiconductor with a large exciton binding energy (60 meV) at room temperature, ZnO nanostructures have been the subject of intensive research [1]. To date, numerous ZnO nanostructures with different sizes and morphologies have been synthesized, including nanowires [2], nanobelts [3], nanocombs [4], nanoshells [5], and tetrapods [6]. The latter is a structure with many promising applications in field emission [7,8], UV and gas sensors [9–13], stimulated emission [14], solar cells [15], and biomedical research [16]. Different sizes and morphologies of the materials have strong effects on their properties and applications. The synthesis of ZnO tetrapods has been achieved through many techniques, including hydrothermal methods [17], thermal evaporation [7–13] and metal organic chemical vapor deposition [18]. Among these methods, the thermal evaporation method is widely employed, as it is simple and highly effective. This method involves the evaporation of metallic Zn in the presence of oxygen [7,19–21] and the carbothermal reduction of a mixture of ZnO and carbon powder under different conditions [22]. The literature has reported that variations in the synthesis conditions, such as the temperature and precursor concentration, in the tube furnace have caused the formation of products with different shapes and size [23–25]. However, systematic studies of the synthetic conditions controlling the growth of tetrapod legs with different morphologies, ranging from uniform diameters to sharp tips, have not yet been published.

Large-scale field-emission devices from ZnO nanoemitters have mainly been fabricated by a screen-printing [26–29] and electrophoretic deposition [30,31]. The former has many technical limitations, including nonuniform dispersion of the emitter particles and low reproducibility. EPD, by contrast, is limited by the emitter non-uniformity, and

*Corresponding author. Tel.: +86 59 122863473.
E-mail address: mla728@hotmail.com (L.A. Ma).

0272-8842/$ - see front matter © 2013 Elsevier Ltd and Techna Group S.r.l. All rights reserved.
http://dx.doi.org/10.1016/j.ceramint.2013.02.027

electrical screening can result in the density of active emitters being low. In the present work, we report for the first time the synthesis of ZnO tetrapods with controlled leg dimensions and morphologies using the thermal evaporation of a surface-modified Zn powder. The correlation between experimental parameters and product morphologies is discussed, and the field emission properties of the ZnO tetrapod films deposited by EPD are investigated.

2. Experimental

2.1. Synthesis of ZnO tetrapods

The synthetic method employed for the ZnO tetrapods in the present work was similar to that reported previously by Kitano et al. [32]. Briefly, Metallic Zn (99.99%) powers were added to an H_2O_2 (0.6%) solution to form a suspension that was vigorously stirred for 60 min. After the suspension was filtered, the resulting Zn powders were poured into a flat pan without covering and dried at 60 °C in air for 6 h. ZnO tetrapods were synthesized in a horizontal electrical furnace [33]. First, the furnace was heated at a rate of 30 °C/min under an argon flow of 300 sccm, and the temperature was maintained at 800–1100 °C. Once the furnace temperature became stable, the surface-modified Zn powders (0.3 g) were placed in a quartz boat and inserted into the tube from the downstream end and placed at the center position of the tube. A small amount of high-purity O_2 gas was then introduced into the reaction tube at ambient pressure. The oxygen gas flow rate was varied from 1 to 10 sccm during the deposition. The details of the deposition process parameters are listed in Table 1. The morphology of the product was examined by scanning electron microscopy (SEM) [Hitachi-S3000N], and the crystal structure of the sample was characterized by X-ray diffraction (XRD) [D/MAX-γA, Cu K_α radiation].

2.2. Preparation of ZnO tetrapod cathodes

The obtained ZnO tetrapods with sharp tips were suitable for field emission. In our experiments, sample 6 (a single morphology with sharp tips, see Table 1) was used as the emitting material. To obtain a stable ZnO tetrapod suspension, which is a prerequisite for EPD, the tetrapods (0.1 g) obtained were first dispersed in DI water by sonication for 30 min. The upper suspension was then used, as it was stable enough for EPD. A small amount of $Mg(NO_3)_2 \cdot 6H_2O$ was added to be used as a charger to render the tetrapod-shaped ZnO particles positively charged. The morphology of the ZnO tetrapod emitters was not changed by the addition of the charger. For EPD, a Ag/ITO coated glass plate was used as the cathode, and a stainless steel plate was used as the anode. These were immersed into the tetrapod suspension, and the two electrodes ($2 \times 2\ cm^2$) were kept at a constant gap of 2 cm. A DC bias of approximately 62 V was applied to the two electrodes for the deposition of the ZnO tetrapod films. The deposition thickness of the tetrapod films was controlled by adjusting the deposition time. After EPD, the cathode was annealed for 30 min at 550 °C. FE measurements were conducted in a vacuum chamber under a pressure of $\sim 10^{-6}$ Torr at room temperature.

Table 1
Deposition parameters of the tetrapods by thermal evaporation.

Sample	O_2 (sccm)	Ar (sccm)	Reaction temperature (°C)	Reaction time (min)
1	5	300	800	5
2	5	300	900	5
3	5	300	1000	5
4	5	300	1100	5
5	1	300	900	5
6	3	300	900	5
7	10	300	900	5

3. Results and discussion

3.1. Effect of growth temperature on the morphology of the tetrapods

The growth of ZnO tetrapods is believed to be dominated by the vapor–solid (VS) process in the thermal evaporation method. The experimental parameters that determine the morphology of the ZnO tetrapod growth include the gas-phase supersaturation [22], the growth temperature [6,12], and the gas flow rate [22]. For the controllable growth of ZnO tetrapods, we kept all other experimental parameters constant and changed the growth temperature. Different morphologies of the ZnO tetrapods were observed with varying growth temperature, as shown in Fig. 1(a)–(d). At a temperature of 800 °C (sample 1), polycrystalline plates on ZnO-tetrapods legs were obtained (Fig. 1(a)). The product collected at 900 °C (sample 2) was in the form of tetrapod-shaped ZnO nanoneedles (Fig. 1(b)). The nanoneedles were typically 500 to 600 nm in diameter at their base and had sharp tips of approximately 50 nm in diameter. The length of the nanoneedles could reach 15 μm. These results are unlike the results of Lee [6], Wan et al. [8] and Dai et al. [20], where there were no reports of tetrapod with sharp tips under this condition. If we increased the temperature to 1000 °C (sample 3), the tetrapods grow longer and larger (Fig. 1(c)), with an average diameter and length of 300 nm and 30 μm, respectively. The observation of large tetrapod crystals is similar to the results reported by Lee [6] and Calestani et al. [11]. It may be noted that higher vaporization temperatures result in longer and larger tetrapods. However, further increases in the temperature to 1100 °C (sample 4) sharply increased the Zn partial pressure,

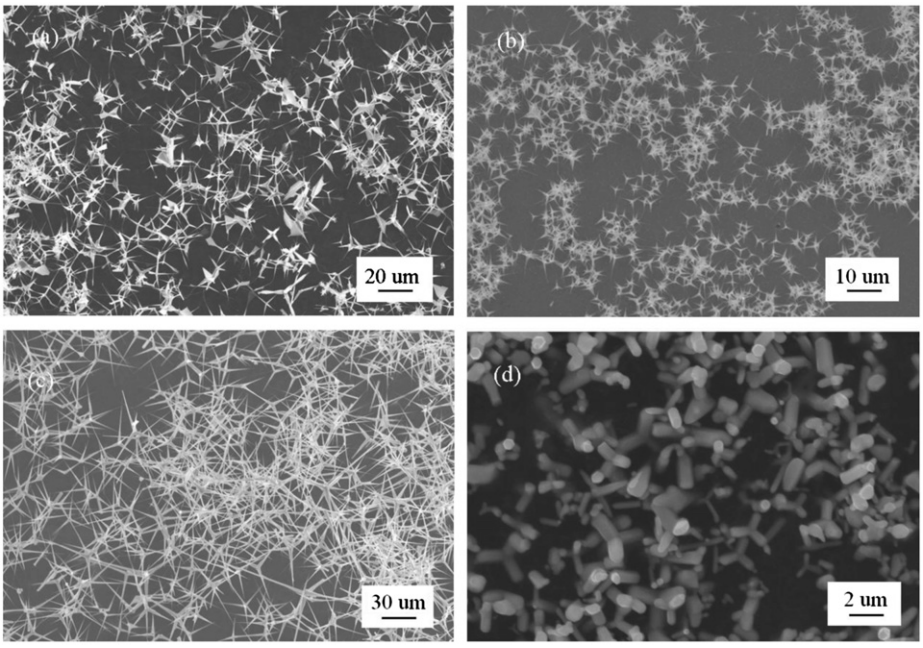

Fig. 1. SEM images showing the tetrapods synthesized under different temperatures with 5 sccm oxygen gas after a growth of 5 min. (a) 800 °C, (b) 900 °C, (c) 1000 °C and (d) 1100 °C.

resulting in drastic changes in the ZnO particle morphology: from tetrapods to irregular nanorods (see Fig. 1(d)). The growth dynamics of the tetrapods in this system are rather complex, and the exact mechanism of growth is not clear. The formation of such highly anisotropic shapes as tetrapods requires a kinetic growth regime in which the rate of the monomer arrival is greater than its diffusion on the surface [34,35]. Under the present conditions, we speculated that the evolution of the legs from nanoneedles to nanorods is a result of a compromise between the preferential growth at the most reactive sites and the enhanced surface diffusion at elevated temperature.

3.2. *Effect of different oxygen flow rates on the morphology of the tetrapods*

Fig. 2 shows the morphologies of the ZnO tetrapods synthesized by vapor deposition at 900 °C with different oxygen flow rates ranging from 1 sccm to 10 sccm. It can be seen from Fig. 2(a)–(f)) that the products are made up of tetrapod structures with high purity. The lengths of the legs are in the range of several μm to more than 20 μm. We found that the morphology of the as-grown tetrapods can be easily adjusted by changing the ratio of oxygen precursor to argon. The product collected in the quartz boat with 1 sccm O_2 (sample 5) was tetrapod nanoneedles (Fig. 2(a)). The length of the nanoneedles reached 3 μm. High-magnification images of the ZnO tetrapods revealed that the nanoneedles had hexagonal cross sections and a layer-stacked structure along the growth direction (Fig. 2(b)), indicating that the growth of the tetrapod nanoneedles followed a VS mechanism [20]. Increasing the oxygen flow rate to 3 sccm (sample 6) led to tetrapods with high aspect ratio legs (diameters 20–300 nm and lengths up to 6 μm), as shown in Fig. 2(c)–(d). When the oxygen flow rate was increased to 5 sccm (sample 2), cotton–wool-like products were formed on the inner walls of the quartz boat. A scanning electron micrograph of this product is shown in Fig. 2(e), revealing tetrapods of 8–15 μm in length. Fig. 2(f) shows a typical enlarged-magnification SEM image of the tetrapod, indicating that the diameter of the tetrapod legs becomes slightly reduced along the growth direction. Interestingly, it was observed that increased oxygen gas flow rates favored the growth of longer ZnO tetrapods. Another derivative of the tetrapods was obtained if the oxygen flow rate was further increased to 10 sccm (sample 7) at 900 °C, as shown in Fig. 3. It can be seen that the legs of different ZnO tetrapods became connected to one another via self-assembly. The growth of connected long-legged tetrapod crystals has been demonstrated previously [36,37]. The terminal-coalescence legs could be initiated by minimizing the deformation energy under suitable growth conditions, as the legs become longer [37].

From the above discussion, we can see that both the temperature and the O_2 flow ratio play important roles in shaping the leg morphologies of ZnO tetrapod nanostructures by changing the surface diffusion conditions and the Zn/O ratio. The conversion efficiency was estimated from the weight of the collected products and the source Zn powder. The efficiency was more than 80% for the Zn source. A representative XRD pattern of the tetrapods is shown in Fig. 4. The diffraction peaks were indexed to

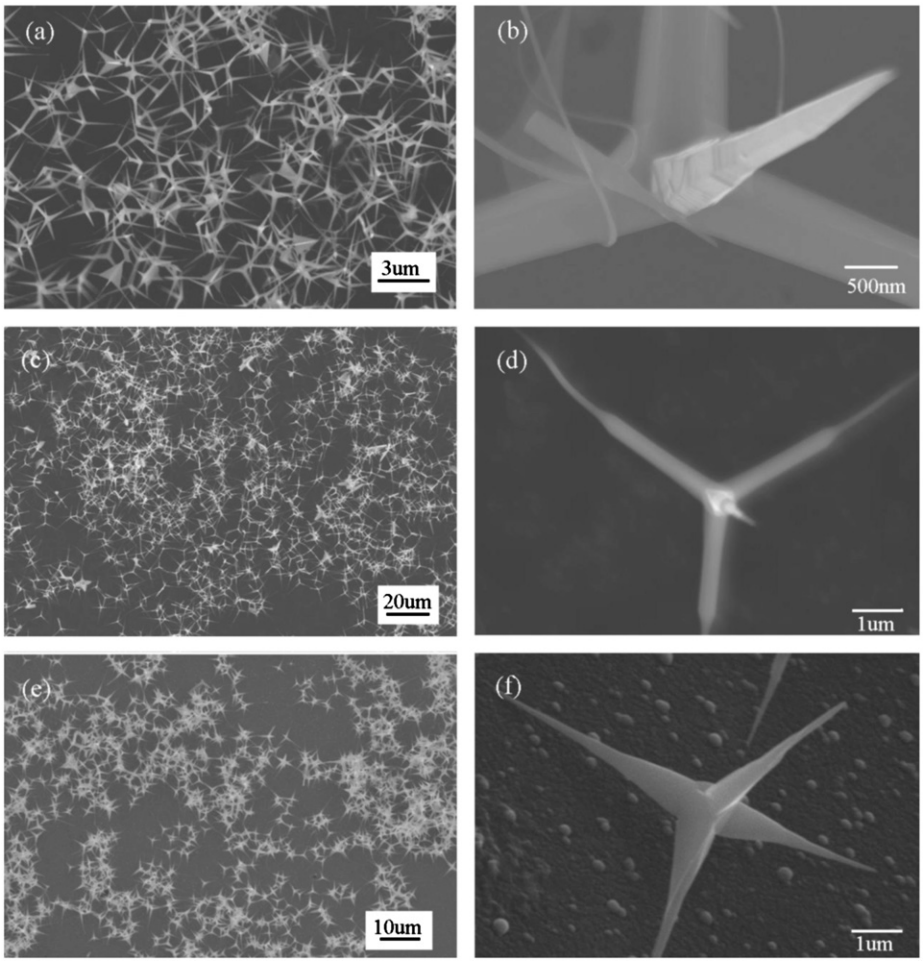

Fig. 2. SEM images of the tetrapods synthesized at 900 °C under different oxygen gas flow rates. (a) 1 sccm, (c) 3 sccm and (e) 5 sccm; (b), (d) and (f) show enlarged-magnification SEM images of the tetrapods.

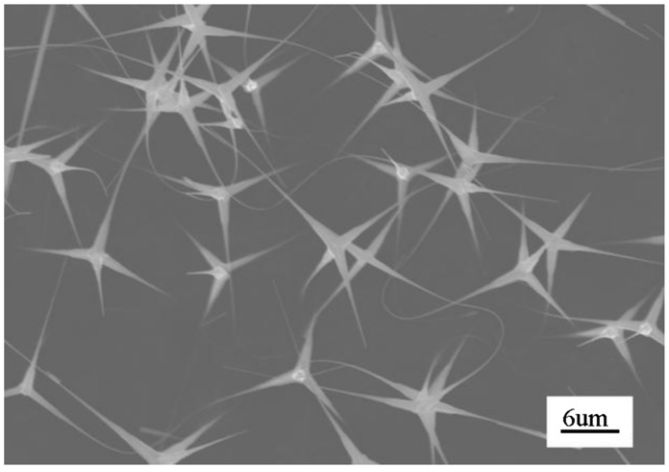

Fig. 3. SEM images of the tetrapods synthesized at 900 °C with 10 sccm oxygen gas.

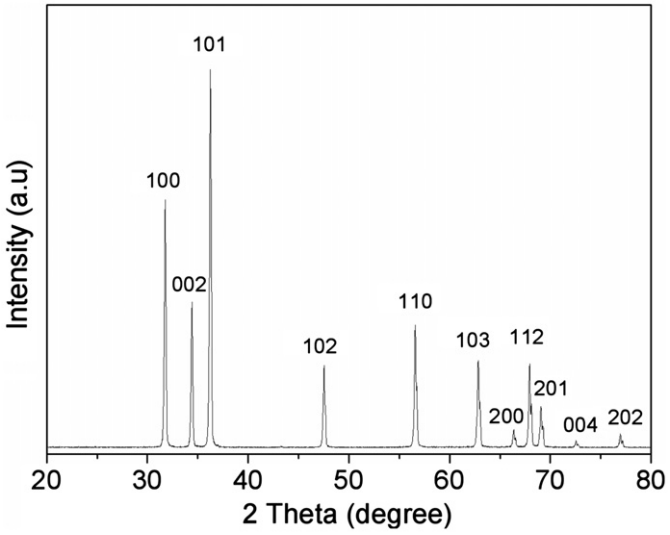

Fig. 4. Typical XRD patterns of the synthesized samples.

(1 0 0), (0 0 2), (1 0 1), (1 0 2), (1 1 0), (1 0 3), (2 0 0), (1 1 2) and (2 0 1), which are attributed to the hexagonal wurtzite structure of ZnO with lattice constants of $a=0.325$ nm and $c=0.521$ nm. No diffraction peaks corresponding to Zn or other impurities were detected. This clearly indicates that the nanostructures grown are of high quality.

3.3. Different deposition times and their effect on the field emission of ZnO tetrapods

Fig. 5(a) shows the FE current density of ZnO tetrapod films with different deposition times versus the electric field (J–E) at a separation of 150 μm between the emitters and the anode. The turn-on field (E_{to}) is defined as the field required at a current density of 10 μA/cm^2 to generate an emission current density. The threshold field (E_{th}) is defined as the field required at a current density of 1 mA/cm^2 to generate an emission current density. It is clear that the tetrapod films deposited for 15 min (sample c) have the best field emission performance with the lowest turn-on field of 1.81 V/μm, the lowest threshold field of 3.82 V/μm, and the highest J at the same E value. The emission current density of the ZnO tetrapods is as high as 1.96 mA/cm^2 at a field of 4.86 V/μm at d=150 μm, indicating efficient field emission from the tetrapod films deposited by electrophoretic deposition. The threshold fields from samples a, b, d and e are 5.57, 4.36, 4.05 and 4.76 V/μm, respectively, as shown in Table 2. We found that the E_{th} value of the ZnO tetrapod cathodes deposited for 10 min was significantly higher than that of the tetrapod-like ZnO wires [7,8,26] or of the aligned ZnO nanowire [38,39] and comparable with that of ZnO nanotetrapods [40]. The field emission data were analyzed using the F–N model [7,39,41].

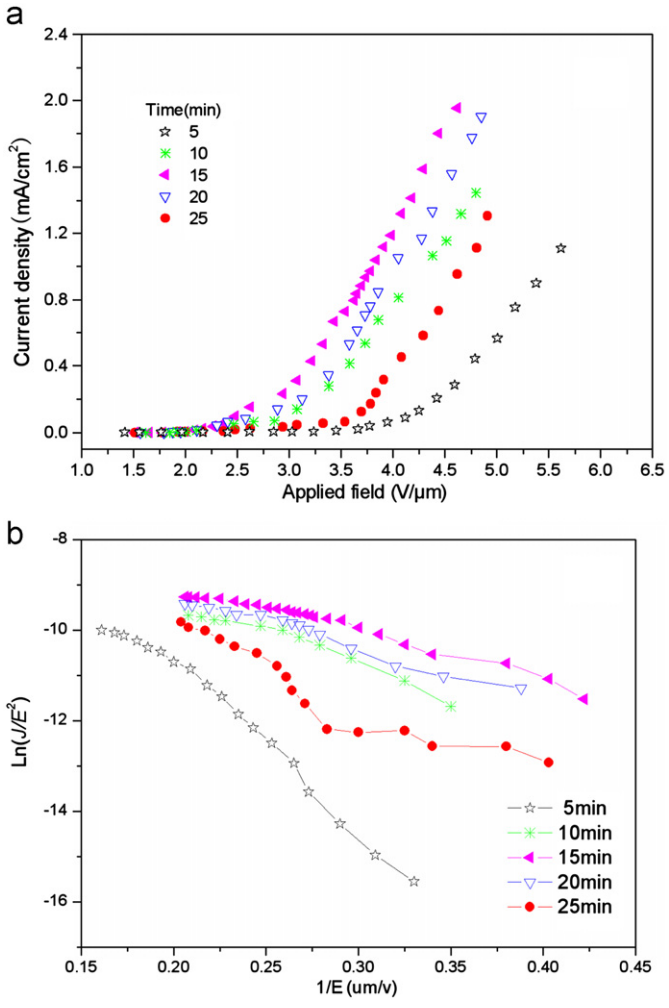

Fig. 5. (a) Field-emission I–V curve from the tetrapod films at different deposited times, and (b) the corresponding F–N plots.

Table 2
Turn-on and threshold fields and β from the tetrapod films of different deposited times.

Sample	Deposition time (min)	Turn-on field (V/μm)	Threshold field (V/μm)	β
a	5	2.62	5.57	3,037
b	10	1.93	4.36	7,262
c	15	1.81	3.82	11,364
d	20	1.87	4.05	8,013
e	25	1.89	4.76	4,256

$$J = (A\beta^2E^2/\phi)\ \exp\ (-B\phi^{3/2}/\beta E) \quad (1)$$

where A and B are constants with values of 1.56×10^{-10} A/V^2/eV and 6.83×10^3 V/eV$^{3/2}$/μm^1, respectively, β is the field enhancement factor, E is the applied electric field, J is the emission current density, and ϕ is the work function of the field material. The data were replotted as ln (I/E^2) versus $1/E$, as shown in Fig. 5(b). The five curves exhibited almost straight lines indicating that the emitting electrons are mainly a result of barrier tunneling electrons extracted by the electric field. Assuming the work function of ZnO to be 5.3 eV [39], the field enhancement factor of the tetrapod films was calculated from the slope (k_{F-N}) according to the equation $k=-B\Phi^{3/2}d/\beta$ [42,43]. The calculated field-enhancement factors (β) from the F–N plots are also summarized in Table 2. It can be seen that sample c has the highest value (11,364) compared to sample a (3037), sample b (7262), sample d (8013), and sample e (4256). This value can be favorably compared with other reported values, which are in the range of 3400–3,3000 [7,8,26,29,40]. According to FN theory, β is strongly dependent on the geometric structure [31,32] (i.e., shape, size, alignment, crystallinity, aspect ratio) and the density of the nanoemitters [42–44] coated on the cathode. In our experiment, the geometry tip size, the crystal structure of the nanostructure and the orientation of the crystals relative to the substrate changed only slightly after deposition, so it is reasonable to assume that density is an important parameter that influences the FE ability of ZnO tetrapod films. For depositions less than 10 min, the samples show poor emission efficiency because there are not enough tetrapod emitters available for effective emission. It is clear that the current density is proportional to the number of the tetrapod emitters; therefore, the field emission of the ZnO tetrapod films in sample c (deposited for 15 min, see Fig. 6(a)) was higher than those in samples a and b. When, the EPD time was increased to 20 min (sample d), the threshold field (E_{th}) and β values were 4.05 V/μm and 8013, respectively. The emission efficiency of sample d was found to be better than

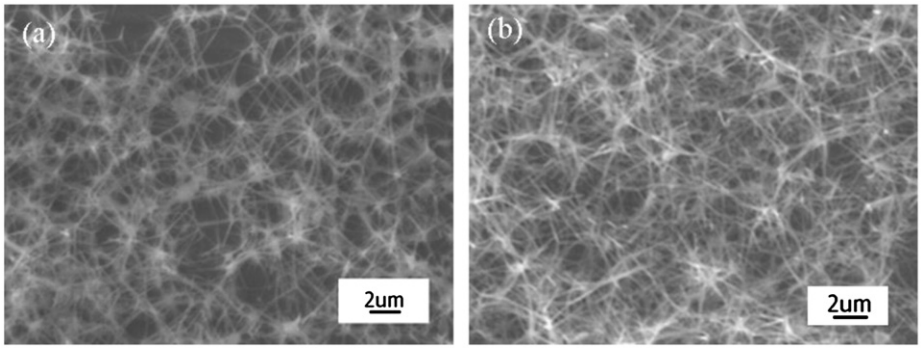

Fig. 6. SEM images of ZnO tetrapods on Ag/ITO coated glass formed by EPD. (a) 15 min, (b) 25 min.

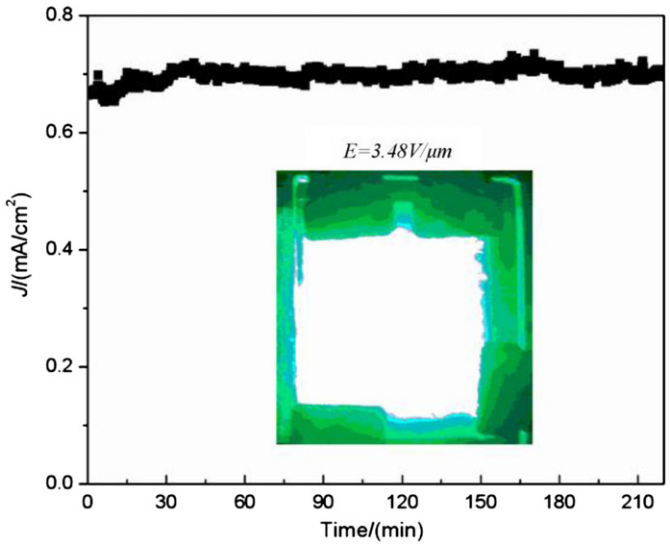

Fig. 7. Stability curve for pre-set values at an applied electric field of approximately 3.48 V/μm and an emitter-anode gap of approximately 150 μm. The inset shows the field emission micrograph of sample c.

that of samples a and b but was lower than that of sample c, which is likely due to the gradual enhancement of screening effects. The emission from sample e is also poor because the densely packed tetrapod films (see Fig. 6(b)) degraded the turn-on field and the FE factor (β). For 15 min ZnO tetrapod films, the excellent field emission properties are likely to be an ideal compromise between the emission current and the β factor.

FE stability measurements were performed on the ZnO tetrapod films (sample c) by maintaining an electric field at 3.48 V/μm over a period of 3 h. No significant degradation of the field emission current was observed. The current fluctuation was lower than 5%, as shown in Fig. 7. A uniform and bright luminescence was observed over the entire field emission area. During these measurements, the brightness and uniformity of the luminescence from the phosphor were maintained, confirming the stability of the FE properties with the ZnO tetrapod field emitter. The observed high stability of the field emission current is ascribed to a little change in the emission site density and a low rate of field evaporation of surface atoms [38], both of which originate from the high physical and chemical stability of the ZnO surface.

4. Conclusion

In summary, ZnO tetrapods with different morphologies were selectively obtained by adjusting the temperature and the ratio of Ar/O_2 during growth. Surface diffusion combined with a preferential growth mechanism was proposed to interpret the morphology evolution of the ZnO tetrapods. In addition, the field emission properties of the ZnO tetrapod films deposited by EPD were first studied, where cathodes deposited for 15 min were found to exhibit the highest emission currents and excellent field emission stability. These results prove that the present tetrapod films are promising candidates for future applications as high brightness electron sources.

Acknowledgments

This work was supported by the Natural Science Foundation of Fujian Province, China (No. 2012J01185) and Fujian University of Technology Foundation, China (No. GY-Z09067, 09061). The authors would like to acknowledge LiQin Hu for SEM and WanYu Wu for valuable discussions regarding FE analysis.

References

[1] Z.L. Wang, Zinc oxide nanostructures: growth, properties and applications, Journal of Physics: Condensed Matter 16 (2004) R829–R858.
[2] S. Rackauskas, A.G. Nasibulin, H. Jiang, Y. Tian, G. Statkute, S.D. Shandakov, H. Lipsanen, E.I. Kauppinen, Mechanistic investigation of ZnO nanowire growth, Applied Physics Letters 95 (2009) 183114.
[3] Z.W. Pan, Z.R. Dai, Z.L. Wang, Nanobelts of semiconducting oxides, Science 291 (2001) 1947–1949.
[4] J.Y. Lao, J.Y. Huang, D.Z. Wang, Z.F. Ren, ZnO nanobridges and nanonails, Nano Letters 3 (2003) 235–238.
[5] Y.H. Leung, K.H. Tam, A.B. Djurisic, M.H. Xie, W.K. Chan, Ding Lu, W.K. Ge, ZnO nanoshells: synthesis, structure, and optical properties, Journal of Crystal Growth 283 (2005) 134–140.

[6] G.H. Lee, Synthesis and cathodoluminescence of ZnO tetrapods prepared by a simple oxidation of Zn powder in air atmosphere, Ceramics International 37 (2011) 189–193.
[7] Y.S. Di, Y.K. Cui, Q.L. Wang, W. Lei, X.B. Zhang, D.D. Engelsen, Field emission from carbon nanotube and tetrapod-like ZnO compound cathode fabricated by spin-coating method, Applied Surface Science 255 (2009) 4636–4639.
[8] Q. Wan, K. Yu, T.H. Wang, C.L. Lin, Low-field electron emission from tetrapod-like ZnO nanostructures synthesized by rapid evaporation, Applied Physics Letters 83 (2003) 2253–2255.
[9] L. Chow, O. Lupan, G.Y. Chai, FIB fabrication of ZnO nanotetrapod and cross-sensor, Physica Status Solidi B Basic Solid State Physics 247 (7) (1628-1632).
[10] O. Lupan, L. Chow, G.Y. Chai, A single ZnO tetrapod-based sensor, Sensors and Actuators B: Chemical 141 (2009) 511–517.
[11] D. Calestani, M. Zha, R. Mosca, A. Zappettini, M.C. Carotta, V. Di Natale, L. Zanotti, Growth of ZnO tetrapods for nanostructure-based gas sensors, Sensors and Actuators B: Chemical 144 (2010) 472–478.
[12] S. Rackauskas, K. Mustonen, T. Järvinen, M. Mattila, O. Klimova, H. Jiang, O. Tolochko, H. Lipsanen, E.I. Kauppinen, A.G. Nasibulin, Synthesis of ZnO tetrapods for flexible and transparent UV sensors, Nanotechnology 23 (2012) 095502.
[13] Z.X. Zhang, L.F. Sun, Y.C. Zhao, Z. Liu, D.F. Liu, L. Cao, B.S. Zou, W.Y. Zhou, C.Z. Gu, S.S. Xie, ZnO tetrapods designed as multiterminal sensors to distinguish false responses and increase sensitivity, Nano Letters 8 (2008) 652–655.
[14] Y.H. Leung, W.M. Kwok, A.B. Djurisic, D.L. Phillips, W.K. Chan, Time-resolved study of stimulated emission in ZnO tetrapod nanowires, Nanotechnology 16 (2005) 579–582.
[15] C.H. Lee, W.H. Chiu, K.M. Lee, W.H. Yen, H.F. Lin, W.F. Hsieh, J.M. Wu, The influence of tetrapod-like ZnO morphology and electrolytes on energy conversion efficiency of dye-sensitized solar cells, Electrochimica Acta 55 (2010) 8422–8429.
[16] L. Nie, L.Z. Gao, P. Feng, J.Y. Zhang, X.Q. Fu, Y.G. Liu, X.Y. Yan, T.H. Wang, Three-dimensional functionalized tetrapod-like ZnO nanostructures for plasmid DNA delivery, Small 2 (2006) 621–625.
[17] C.Y. Liu, H.Y. Li, W.Q. Jie, X.Z. Zhang, D.P. Yu, Preparation of ZnO cluster and rod-like whiskers through hydrothermal methods, Materials Letters 60 (2006) 1394–1398.
[18] H.J. Kim, K. Sung, K.S. An, Y.K. Lee, C.G. Kim, Y.H. Lee, Y. Kim, ZnO nanowhiskers on ZnO nanoparticles-deposited Si (1 1 1) by MOCVD, Journal of Materials Chemistry 14 (2004) 3396–3397.
[19] G.H. Lee, Optimal Zn/O ratio in vapor phase for the synthesis of high quality ZnO tetrapod nanocrystals via thermal evaporation of Zn in Air, Applied Surface Science 259 (2012) 562–565.
[20] Y. Dai, Y. Zhang, Q.K. Li, C.W. Nan, Synthesis and optical properties of tetrapod-like zinc oxide nanorods, Chemical Physics Letters 358 (2002) 83–86.
[21] J.J. Delaunay, N. Kakoiyama, I. Yamada, Fabrication of three-dimensional network of ZnO tetratpods and its response to ethanol, Materials Chemistry and Physics 104 (2007) 141–145.
[22] Y.G. Wang, M. Sakurai, M. Aono, Mass production of ZnO nanotetrapods by a flowing gas phase reaction method, Nanotechnology 19 (2008) 245610.
[23] V.A.L. Roy, A.B. Djurisic, W.K. Chan, J. Gao, H.F. Lui, C. Surya, Luminescent and structural properties of ZnO nanorods prepared under different conditions, Applied Physics Letters 83 (2003) 141–143.
[24] C.Y. Leung, A.B. Djurisic, Y.H. Leung, L. Ding, C.L. Yang, W.K. Ge, Influence of the carrier gas on the luminescence of ZnO tetrapod nanowires, Journal of Crystal Growth 290 (2006) 131–136.
[25] Z.G. Chen, A. Ni, F. Li, H. Cong, H.M. Cheng, G.Q. Lu, Synthesis and photoluminescence of tetrapod ZnO nanostructures, Chemical Physics Letters 434 (2007) 301–305.
[26] K. Hou, C. Li, W. Lei, X.B. Zhang, K. Qu, X.X. Yang, Z.W. Zhao, B.P. Wang, Stable field emission from screen-printed ZnO-tetrapod emitters, Journal of Vacuum Science and Technology B 26 (2008) 1305–1308.
[27] X.M. Fan, H.G. Zhang, J. Wang, Z.W. Zhou, Influence of annealing temperature on field emission from tetrapod-shaped ZnO-whisker films obtained by screen printing, Materials Science in Semiconductor Processing 13 (2010) 400–404.
[28] L.M. Yu, X.H. Fan, L.J. Qi, W. Yan, Field emission property of printed CNTs-mixed ZnO nanoneedles, Applied Surface Science 257 (2011) 6332–6335.
[29] Y.K. Cui, X.B. Zhang, W. Lei, Y.S. Di, M. Xiao, X.X. Yang, Z.W. Zhao, ZnO nanostructures and its influence on the field-emission performance, IEEE Electron Device Letters 31 (2010) 479–481.
[30] Z.X. Lin, T.L. Guo, Tetrapod-like nano ZnO field emission display with triode structure, Acta Optica Sinica 29 (2009) 500–505.
[31] L.M. Yu, C.C. Zhu, Field emission characteristics study for ZnO/Ag and ZnO/CNTs composites produced by DC electrophoresis, Applied Surface Science 255 (2009) 8359–8362.
[32] M. Kitano, T. Hamabe, S. Maeda, T. Okabe, Growth of large tetrapod-like ZnO crystals: I. Experimental considerations on kinetics of growth, Journal of Crystal Growth 102 (1990) 965–973.
[33] L.A. Ma, Z.X. Lin, J.Y. Lin, Y.A. Zhang, L.Q. Hu, T.L. Guo, Large-scale growth of ultrathin MgO nanowires and evaluate their field emission properties, Physica E: Low-dimensional Systems and Nanostructures 41 (2009) 1500–1503.
[34] Y. Yin, A.P. Alivisatos, Colloidal nanocrystal synthesis and the organic-inorganic interface, Nature 437 (2005) 664–670.
[35] J. Watt, N. Young, S. Haigh, A. Kirkland, R.D. Tilley, Synthesis and structural characterization of branched palladium nanostructures, Advanced Materials 21 (2009) 2288–2293.
[36] L.B. Feng, A.H. Liu, M. Liu, Y.Y. Ma, J. Wei, B.Y. Man, Fabrication and characterization of tetrapod-like ZnO nanostructures prepared by catalyst-free thermal evaporation, Materials Characterization 61 (2010) 128–133.
[37] Y.N. Zhao, M.S. Cao, J.G. Li, Y.J. Chen, A novel and simple combustion route towards long legs nanotetrapod ZnO, Materials Research Bulletin 40 (2005) 1745–1750.
[38] V. Semet, Th. Vu Thien Binh, L. Pauporte, Joulaud, F.J. Vermersch, Field emission behavior of vertically aligned ZnO nanowire planar cathodes, Journal of Applied Physics 109 (2011) 054301.
[39] C.J. Lee, T.J. Lee, S.C. Lyu, Y. Zhang, H. Ruh, H.J. Lee, Field emission from well-aligned zinc oxide nanowires grown at low temperature, Applied Physics Letters 81 (2002) 3648–3650.
[40] C. Li, K. Hou, X.X. Yang, K. Qu, W. Lei, X.B. Zhang, B.P. Wang, X.W. Sun, Enhanced field emission from ZnO nanotetrapods on a carbon nanofiber buffered Ag film by screen printing, Applied Physics Letters 93 (2008) 233508.
[41] J.C. She, Z.M. Xiao, Y.H. Yang, S.Z. Deng, J. Chen, G.W. Yang, N.S. Xu, Correlation between resistance and field emission performance of individual ZnO one-dimensional nanostructures, ACS Nano 2 (2008) 2015–2021.
[42] N.S. Liu, G.J. Fang, W. Zeng, H. Zhou, H. Long, X.Z. Zhao, Enhanced field emission from three-dimensional patterned carbon nanotube arrays grown on flexible carbon cloth, Journal of Materials Chemistry 22 (2012) 3478–3484.
[43] K.J. Huang, Y.S. Hsiao, W.T. Whang, Selective growth and enhanced field emission properties of micropatterned iron phthalocyanine nanofiber arrays, Organic Electronics 12 (2011) 1826–1834.
[44] S.M. Pimenov, V.D. Frolov, A.V. Kudryashov, M.M. Lamanov, N.P. Abanshin, B.I. Gorfinkel, D.W. Kim, Y.J. Choi, J.H. Park, J.G. Park, Electron field emission from semiconducting nanowires, Diamond and Related Materials 17 (2008) 758–763.